Supporting Information for

Accessing New Microporous Polybifluorenes Via a C/Si Switch

Andrei Nesmelov,[a] David Lee,[a] Christopher Bejger,[a] Margaret Kocherga,[a] Zachary Lyles,[a] Madeline Greenier,[a] Ashley Ariel Vitallo, [a] Ghallia Kaouk,[a] Daniel Jones,[a] Thomas A. Schmedake[a]

Table of Contents

Instrumentation and synthetic details	2-4
Adsorption isotherm data	5-6
FTIR spectra	7-8
NMR spectra	9-14
Solid state NMR	15
Powder XRD	16
Diffuse Reflectance UV-Vis	17
Fluorescence Quenching – Stern-Volmer Plots	18
Quenching mechanism studies	19-24
SEM	25
Computational modeling	26-28
X-ray Crystal Data for **1** and **2**	29-30
References	31

[a.] *Department of Chemistry, University of North Carolina – Charlotte, Charlotte, NC 28223, USA. Email:Tom.Schmedake@uncc.edu*

Instrumentation and General Methods

Fluorescence measurements were conducted on a Jobin-Yvon Fluorolog 3 fluorescence spectrometer. NMR spectra were acquired using a JEOL 300 MHz and a 500 MHz NMR spectrometer. Solid state NMR experiments were conducted at the University of South Carolina – Columbia on a Bruker Avance III-HD 500 MHz NMR with magic angle spinning. Combustion analysis (C, H, and N) was conducted by Atlantic Microlab, Inc. FTIR spectra were obtained with a PerkinElmer Specturm 100 FTIR with Universal ATR Sampling Accessory. UV-vis data were acquired with a Cary 5000 spectrometer and a Harrick Cricket DRUV accessory with specular reflectance blocked. Powder XRD was acquired with a PANalytical's X'Pert PRO Materials Research Diffractometer.

Nitrogen adsorption isotherms were determined using a NOVA 2200e Quantachrome surface area and pore size analyzer. Due to the microporous nature of the material, additional adsorption data points were obtained at very low P/P_o levels to obtain the BET surface area following the recommended criteria for microporous surface area determination:[1]

(a) C should be positive

(b) application of the BET equation should be restricted to the range where the term $n(1 - P/P_o)$ continuously increases with P/P_o

(c) the P/P_o value corresponding to nm should be within the selected BET range

X-ray crystallography data were acquired with an Agilent (now Rigaku) Gemini A Ultra diffractometer. Crystals of suitable size were coated with a thin layer of paratone-N oil, mounted on the diffractometer, and flash cooled to 105 K in the cold stream of the Cryojet XL liquid nitrogen cooling device (Oxford Instruments) attached to the diffractometer. The diffractometer was equipped with sealed-tube long fine focus X-ray sources with Mo target (λ = 0.71073 Å) and Cu target (λ = 1.5418 Å), four-circle kappa goniometer, and CCD detector. CrysAlisPro[2] software was used to control the diffractometer and perform data reduction. The crystal structure was solved with SHELXS.[3] All non-hydrogen atoms appeared in the E-map of the correct solution. Alternate cycles of model-building in Olex2[4] and refinement in SHELXL[3] followed. All non-hydrogen atoms were refined anisotropically. All hydrogen atom positions were calculated based on idealized geometry and recalculated after each cycle of least squares. During refinement, hydrogen atom – parent atom vectors were held fixed (riding motion constraint).

Experimental

Materials: Bis(1,5-cyclooctadiene)nickel(0), 98%, $Ni(COD)_2$ and 2,2'-bipyridine, 99+%,were purchased from Alfa Aesar and used without further purification. N,N-Dimethylformamide, anhydrous ≥ 99.8%, DriSolv® was purchased from Millipore Sigma and used without further purification. 2,2',7,7'- Tetrabromospirobifluorene, 95%, was purchased from Sigma-Aldrich and used as obtained without further purification. 5,5'-Dibromo-2,2'-diiodo-1,1'-biphenyl and 4,4'-dibromo-2,2'-diiodo-1,1'-biphenyl were synthesized following literature procedures.[5,6]

Synthesis of 2,2',7,7'-tetrabromospirosilabifluorene, 1

A 100 ml three neck round bottom flask was charged with 3.00 g 4,4'-dibromo-2,2'-diiodobiphenyl (5.32 mmol) and 60 mL dry THF. The solution was subjected to three freeze pump thaw cycles and cooled to -90 °C. 4.84 mL n-BuLi (2.2M in hexanes, 10.6 mmol) was added dropwise via syringe. The reaction was stirred at this temperature for one hour, and 0.6 ml $SiCl_4$ (0.5 mmol) was added dropwise. The reaction was allowed to warm to room temperature and stirred overnight. 100 mL H_2O was added to the solution and the resulting mixture was extracted with diethyl ether (3 x 100 mL). The organic layer was dried with $MgSO_4$, filtered, and evaporated to dryness to yield a yellow/orange solid. The crude product was rinsed thoroughly with cold dichloromethane to yield 0.95 g product as a white powder (55%). Crystals suitable for X-ray analysis were grown via evaporation of a toluene solution at room temperature. ^{1}H NMR ($CDCl_3$, 300 MHz): δ = 7.75 (d, 4 H, J = 8.4 Hz), 7.65 (d,d 4 H, , J = 8.4 Hz, 2.1 Hz), 7.50 (d, 4 H, J = 2.1 Hz); ^{13}C NMR ($CDCl_3$, 75 MHz): δ = 147.7, 137.0, 135.0, 133.3, 123.2, 123.0 ppm; ^{29}Si NMR ($CDCl_3$, 99 MHz): δ = -7.32 ppm. MS(EI): m/z = 647.7 (M+). Elemental analysis calcd. (%) for $C_{24}H_{12}Br_4Si$: C 44.48, H 1.87, N 0; found: C 44.55, H 1.84, N 0.0.

Synthesis of 3,3',6,6'-tetrabromo-spirosilabifluorene, 2

3.00 g 5,5'-dibromo-2,2'-diiodobiphenyl (5.32 mmol) was substituted into the procedure for **1**, keeping all the same conditions. The crude product was rinsed thoroughly with dichloromethane to yield 0.88 g product as a white powder (51%). Crystals for X-ray analysis were grown via evaporation of a filtered ethyl acetate solution at room temperature. ^{1}H NMR ($CDCl_3$, 300 MHz): δ = 8.01 (d, 4 H, J =1.5 Hz), 7.40 (d,d 4 H, J = 7.5 Hz, 1.5 Hz), 7.24 (d, 4 H, , J = 7.5 Hz); ^{13}C NMR ($CDCl_3$, 75 MHz): δ = 150.6, 135.6, 131.7, 130.3, 127.3, 125.0 ppm; ^{29}Si NMR ($CDCl_3$, 99 MHz): δ = -6.90 ppm. MS (EI): m/z = 647.7 (M+). Elemental analysis calcd. (%) for $C_{24}H_{12}Br_4Si$: C 44.48, H 1.87, N 0; found: C 44.46, H 1.71, N 0.0.

Yamamoto coupling, general procedure

Yamamoto coupling of **1**, **1-C**, and **2**, to **PS1, PS1-C**, and **PS2** was accomplished using the procedure described by Hauser and coworkers.[7] 2,2'-Bipyridine (0.253 g, 1.6 mmol) was added to a 100 mL round bottom flask under nitrogen atmosphere. 1.5-Cyclooctadiene (0.195 mL, 1.6 mol) was added to the flask. Anhydrous DMF (60 mL) was added to the flask. The flask was sparged with nitrogen for a half hour. $Ni(COD)_2$ (0.429 g., 1.6 mmol) was dissolved in dry DMF (25 mL) under nitrogen atmosphere. The two mixtures were combined in a single flask under nitrogen. The resulting mixture was heated to 85 ^oC for two hours. After heating, the mixture was transferred via cannula to a flask containing **1**, **1-C**, or **2**, (0.200 g) and was stirred at 85 ^oC for 16 hours. The mixture was cooled in an ice bath and quenched with concentrated HCl. The solid product was removed by filtration and washed with DMF (three times), water (three times), and acetone (three times), then the sample was dried overnight in a vacuum oven.

PS1-C[7]

Yield: 0.186 g 97%, based on $C_{25}H_{12}$. Elemental analysis calculated range (%) for $C_{25}H_{16}$ – $C_{25}H_{12}$: C 94.9-96.13, H 5.1-3.87, N 0; found (comb. anal.): C 93.1, H 4.5, N 0.4. Note previously reported combustion analysis results for **PS1-C** were also lower than predicted (C 89.3, H 4.2, N 0.2), which was attributed by the authors to incomplete combustion.

PS1

Yield: 0.185 g, 92% based on $C_{24}H_{12}Si$. Elemental analysis calculated range (%) for $C_{24}H_{16}Si$ – $C_{24}H_{12}Si$: C 86.70-87.77, H 4.85-3.68, Si:8.45-8.55, N 0; found (comb. anal.): C 80.9, H 4.4, N 0.0; found (EDAX): Si 6.4.

PS2

The Yamamoto coupling procedure was performed as described above but at half scale using 0.100 g of **2**. Yield: 0.092 g, 91 % based on $C_{24}H_{12}Si$. Elemental analysis calculated range (%) for $C_{24}H_{16}Si$ – $C_{24}H_{12}Si$:C 86.70-87.77, H 4.85-3.68, Si:8.45-8.55, N 0; found (comb. anal.): C 81.8, H 4.4, N 0.4; found (EDAX): Si 6.8.

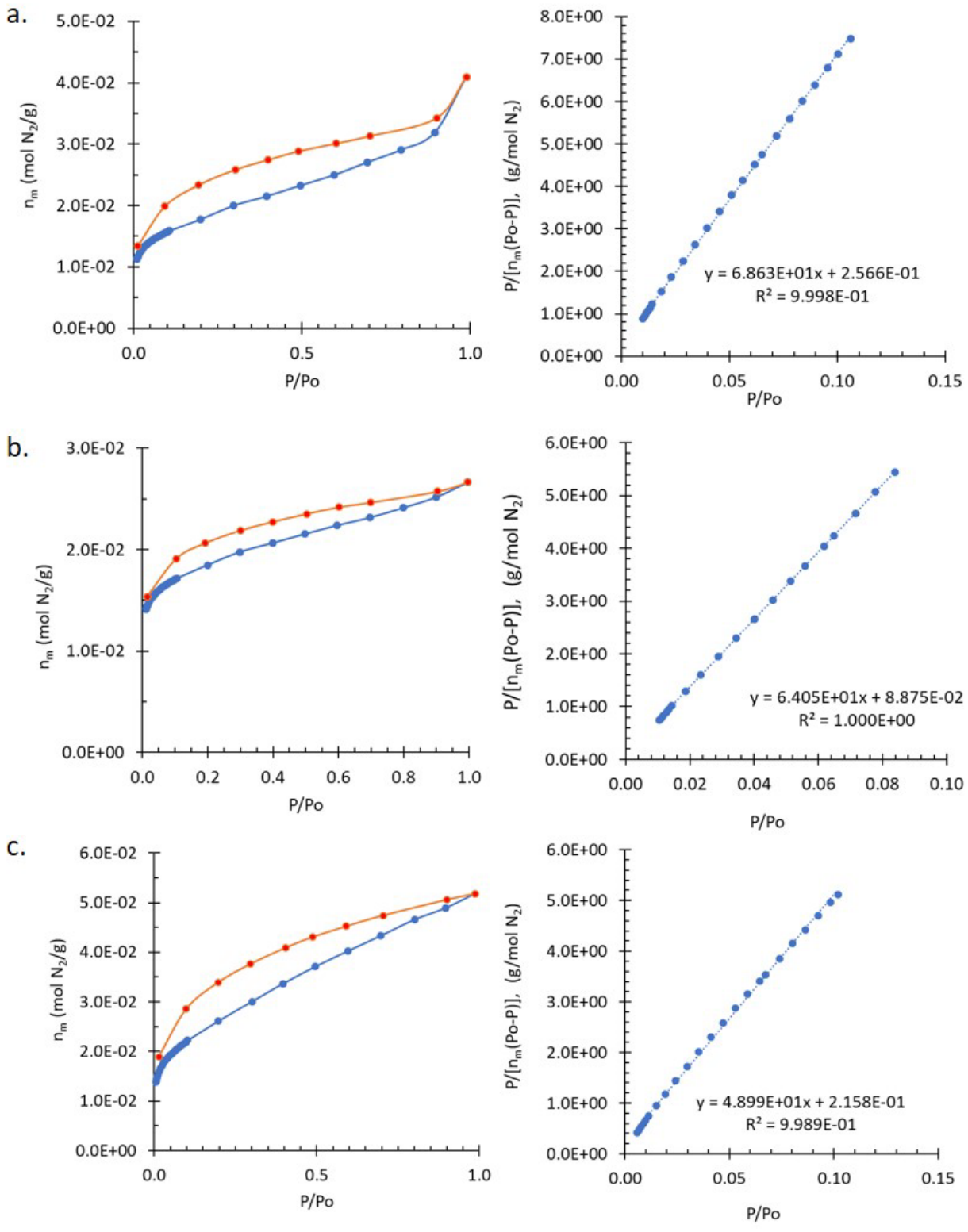

Figure S1. (Left) Adsorption (blue) and desorption (red) isotherms and (right) BET transform plots for (a) **PS1**, (b) **PS2**, and (c) **PS1-C**.

Table S1. Results from BET transform of adsorption isotherm data.

Sample	Slope	Intercept	Correlation constant (r^2)	C	n_m, (mol N_2/g)	Surface Area (m^2/g)
PS1	6.86E1	2.57E-1	1.000	268	1.45E-2	1420
PS2	6.41E1	8.88E-2	1.000	723	1.56E-2	1520
PS1-C	4.90E1	2.16E-1	0.999	228	2.03E-2	1980

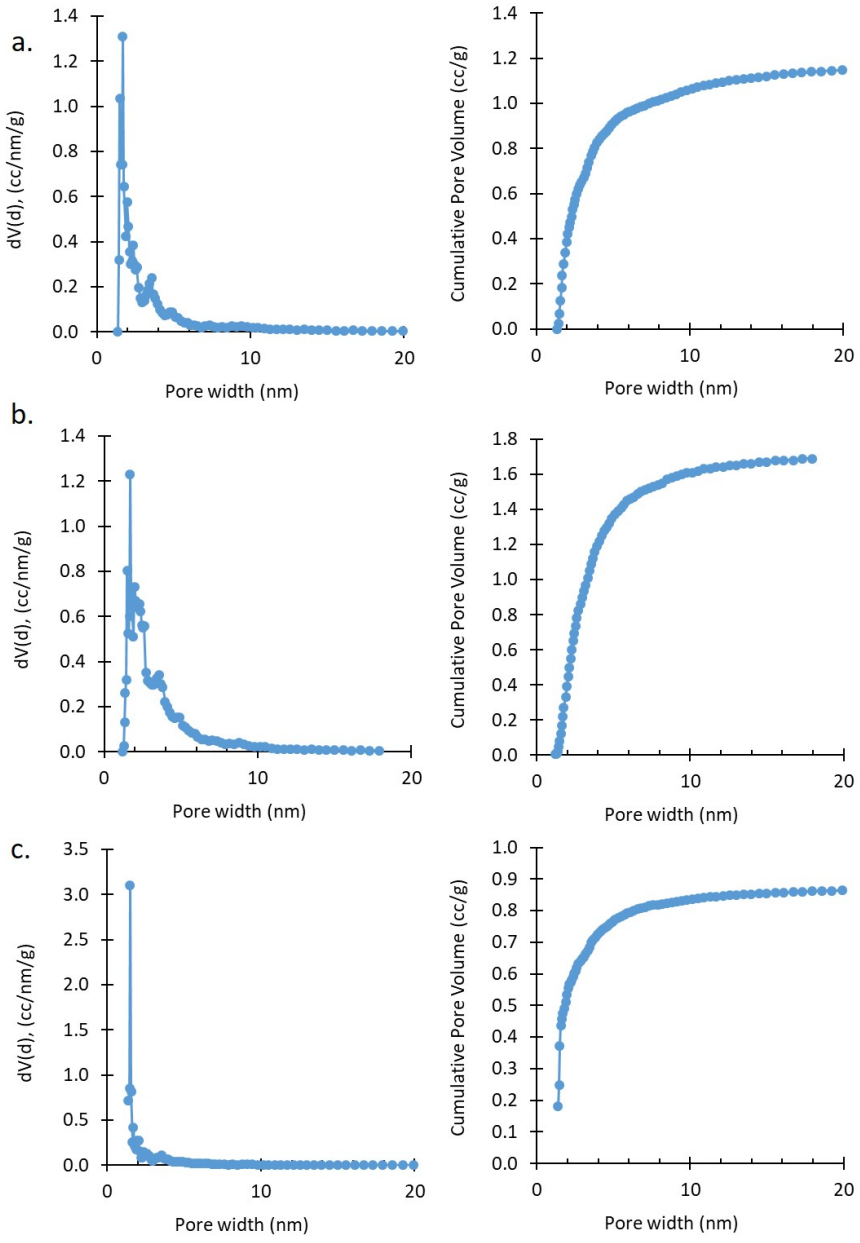

Figure S2. Pore size analysis for (a) **PS1**, (b) **PS1-C**, and (c) **PS2**. Calculation model: N_2 at 77 K on carbon (cylindrical pores, NLDFT equilibrium model, Quantachrome NovaWin)

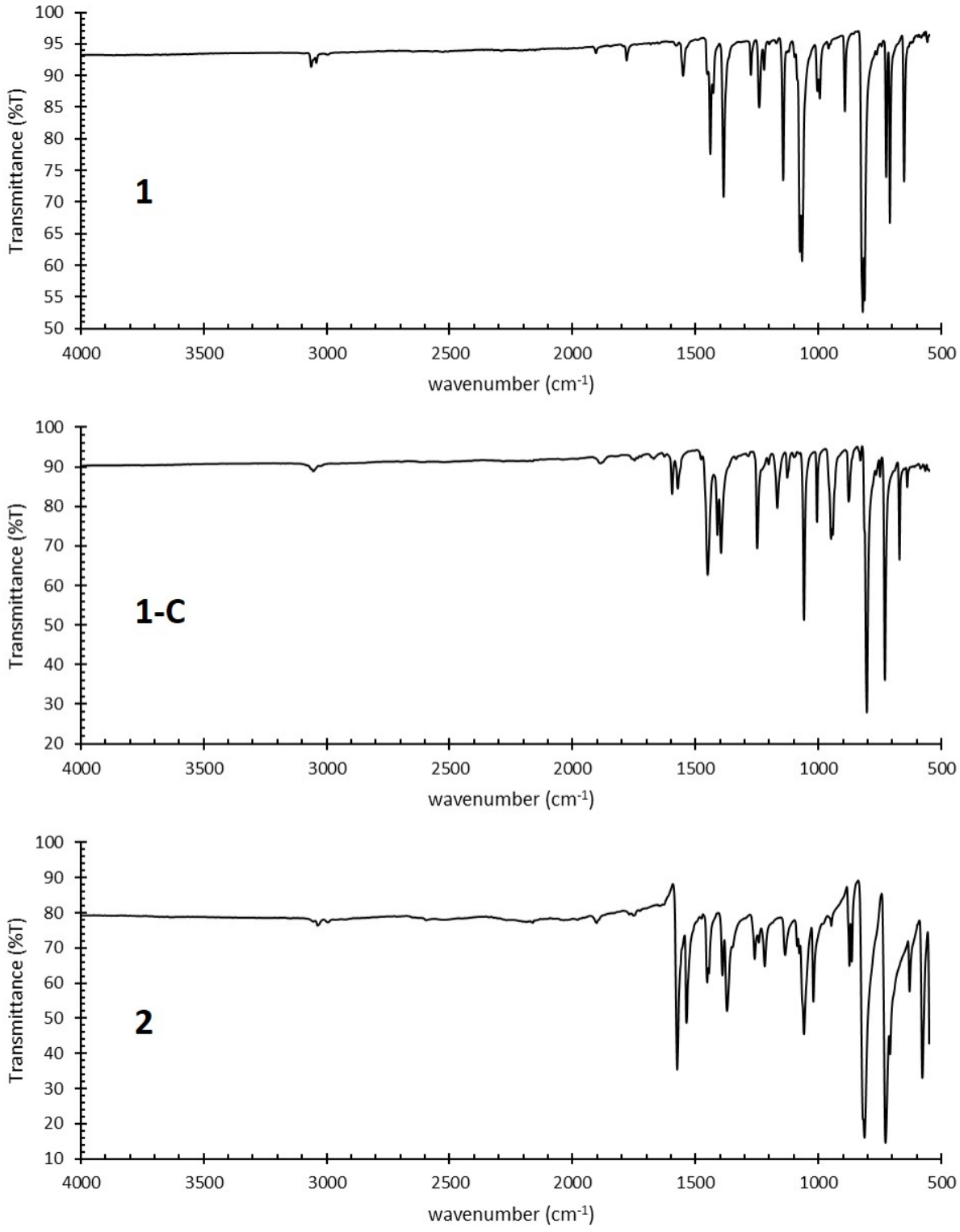

Figure S3. FTIR spectra of compounds **1**, **1-C**, and **2**.

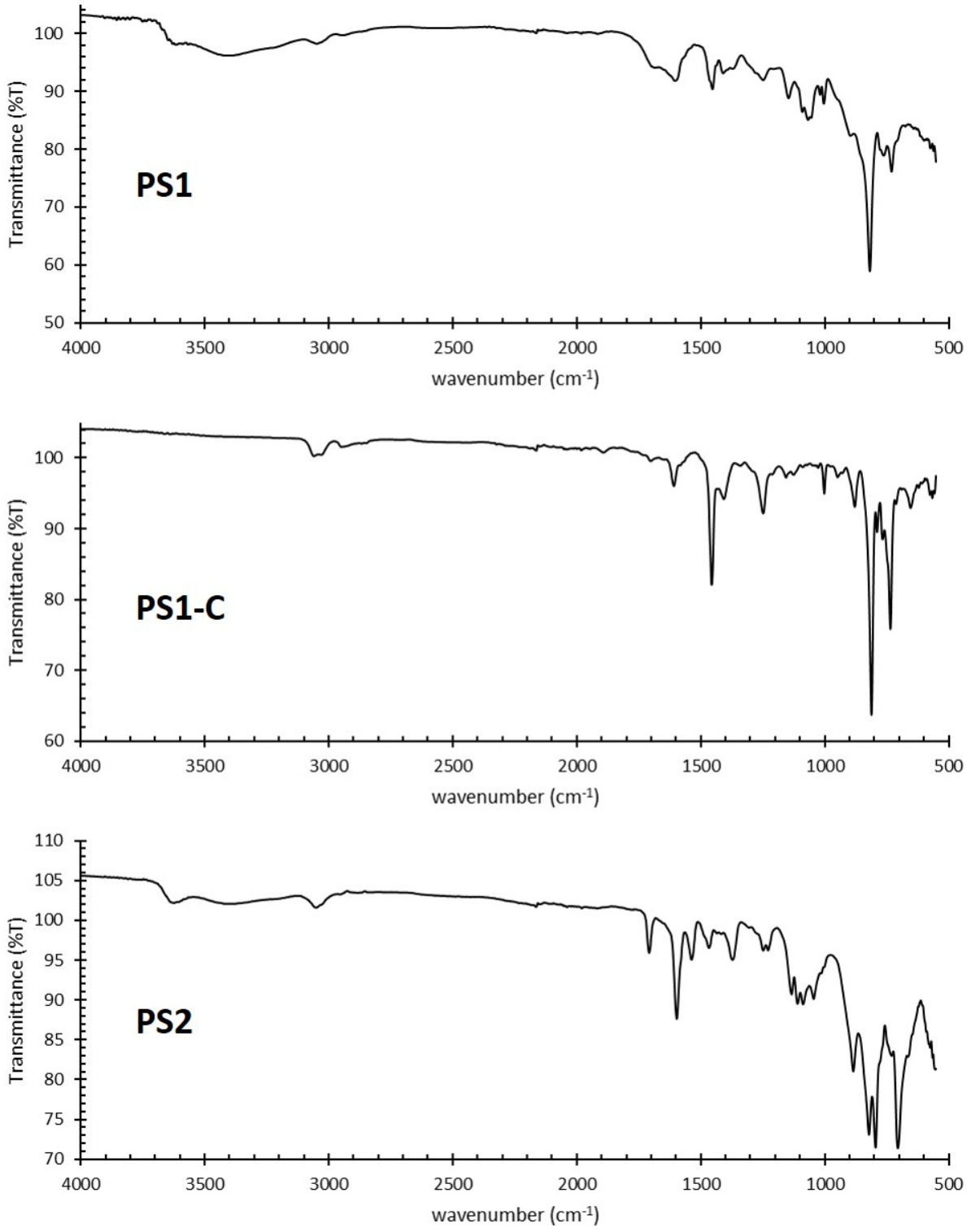

Figure S4. FTIR spectra of polymers **PS1**, **PS1-C**, and **PS2**.

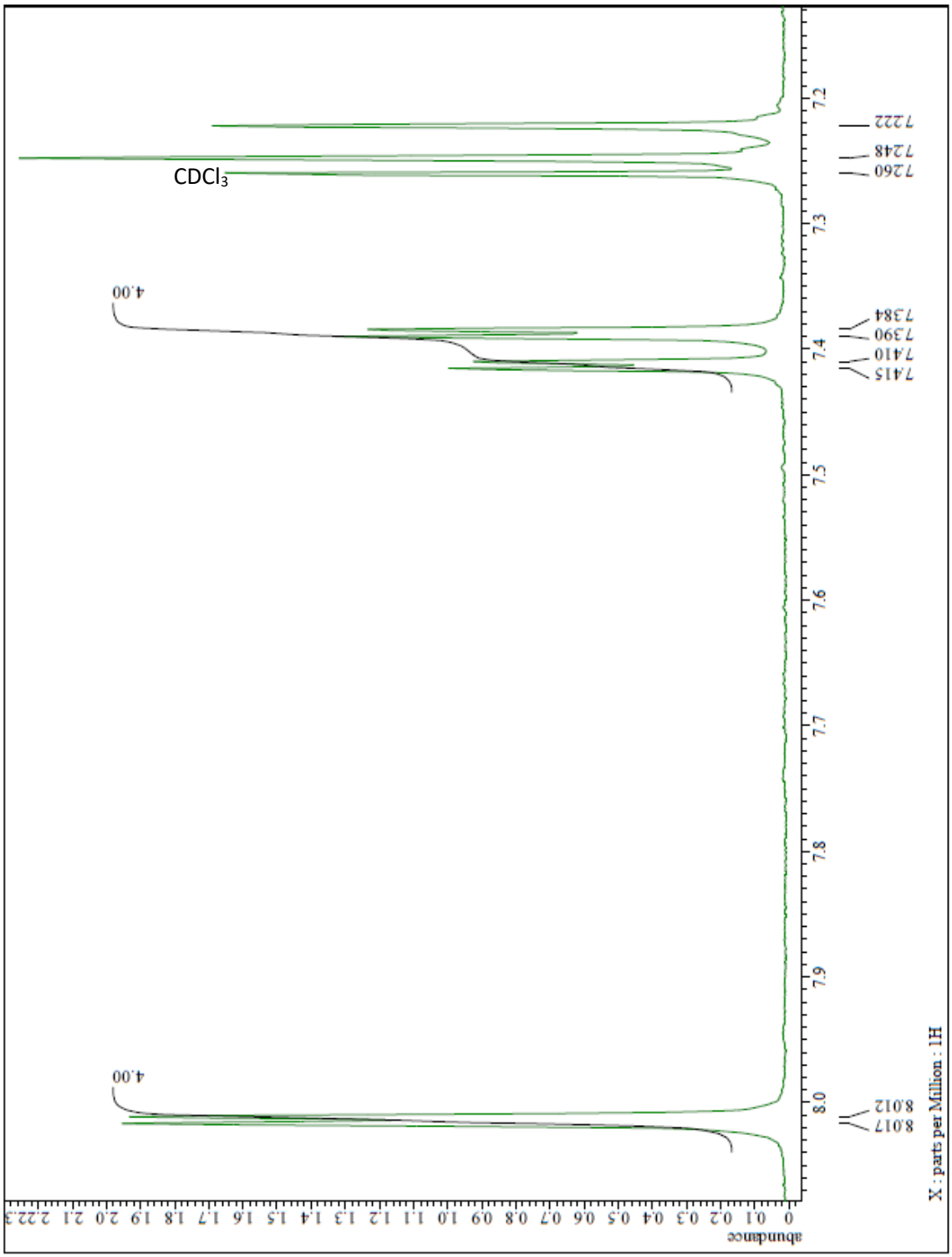

Figure S5. ^{1}H-NMR (300 MHz, $CDCl_3$) of **2**

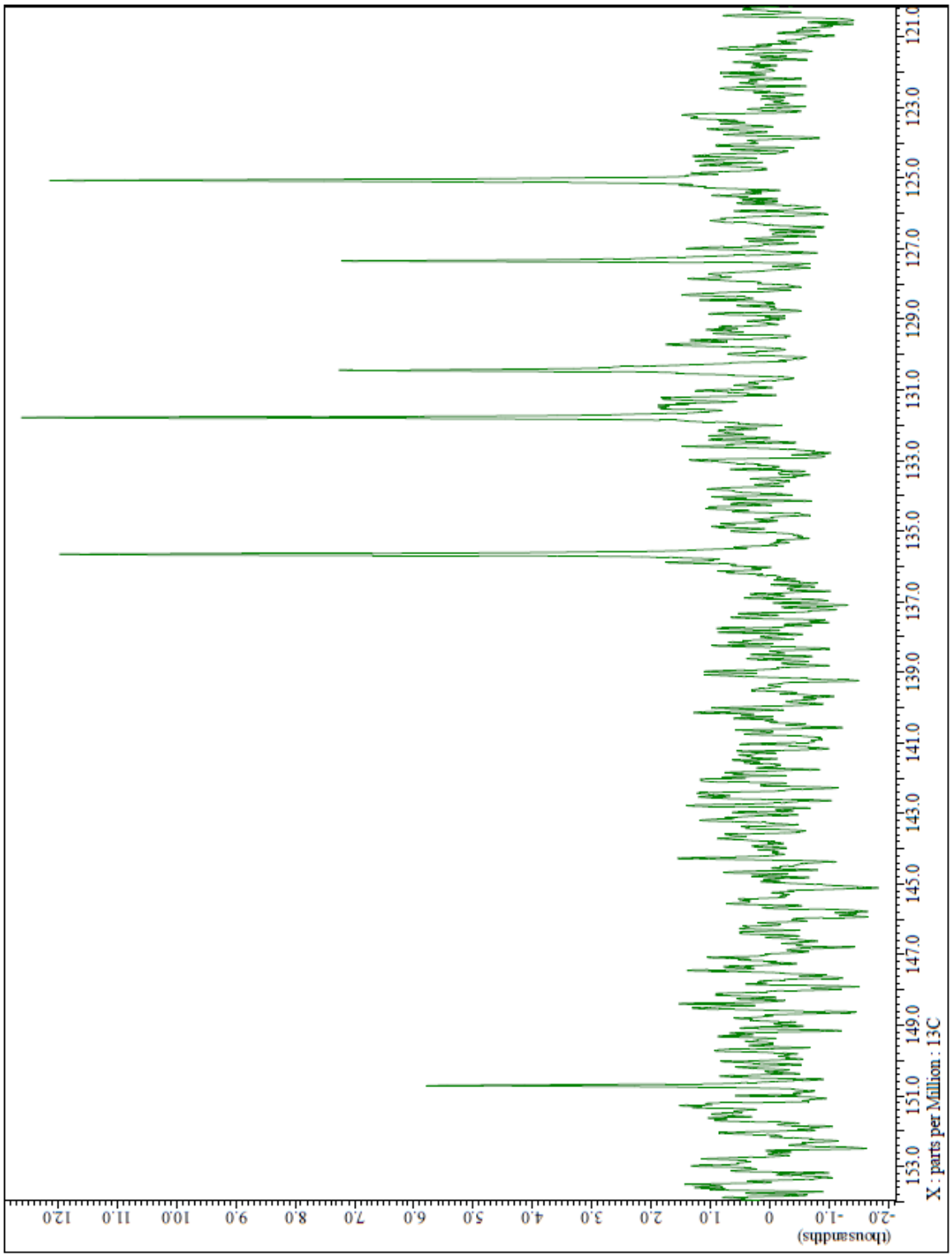

Fig. S6. ^{13}C-NMR (300 MHz, $CDCl_3$) of **2**

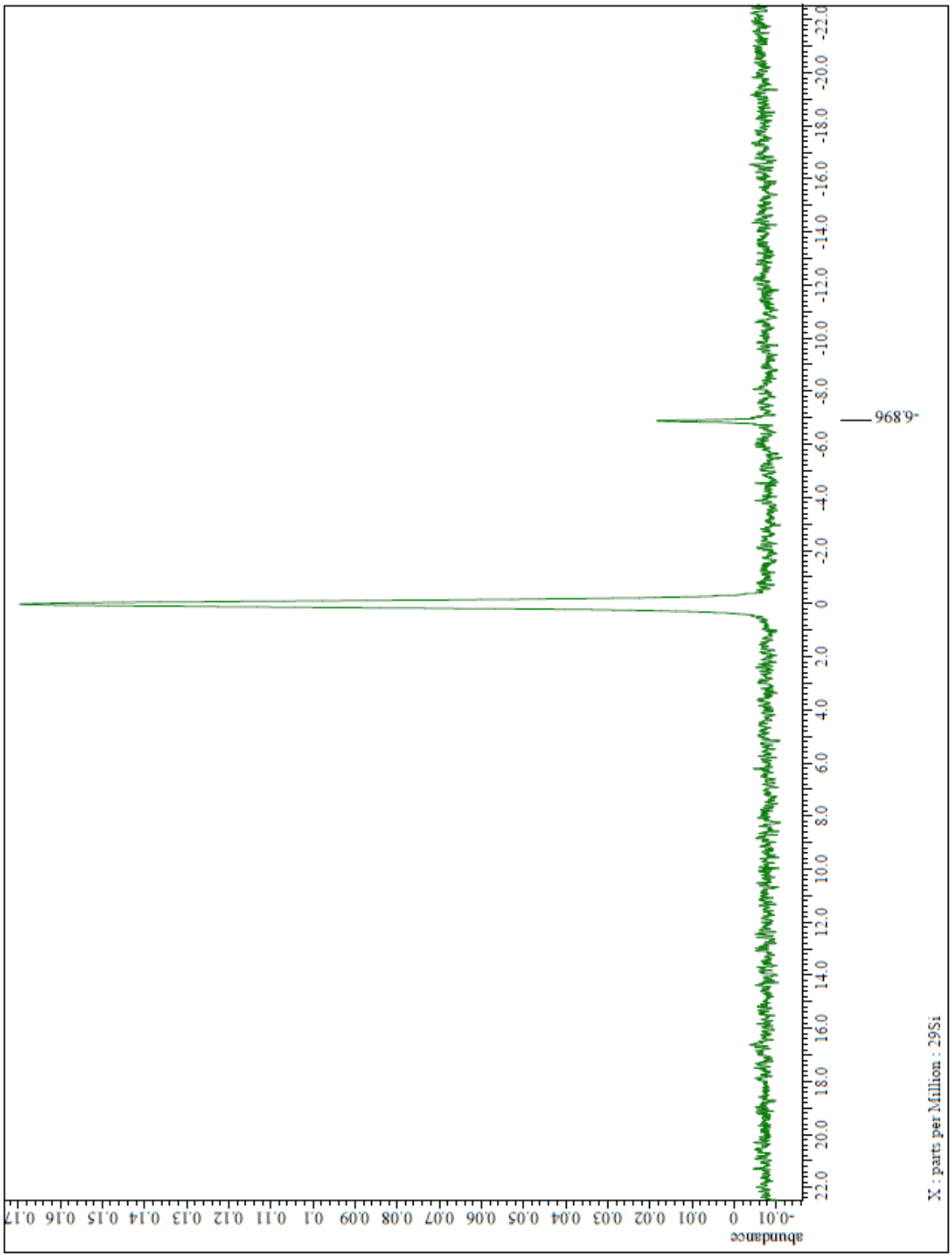

Figure S7. ^{29}Si-NMR (500 MHz, $CDCl_3$) of **2**

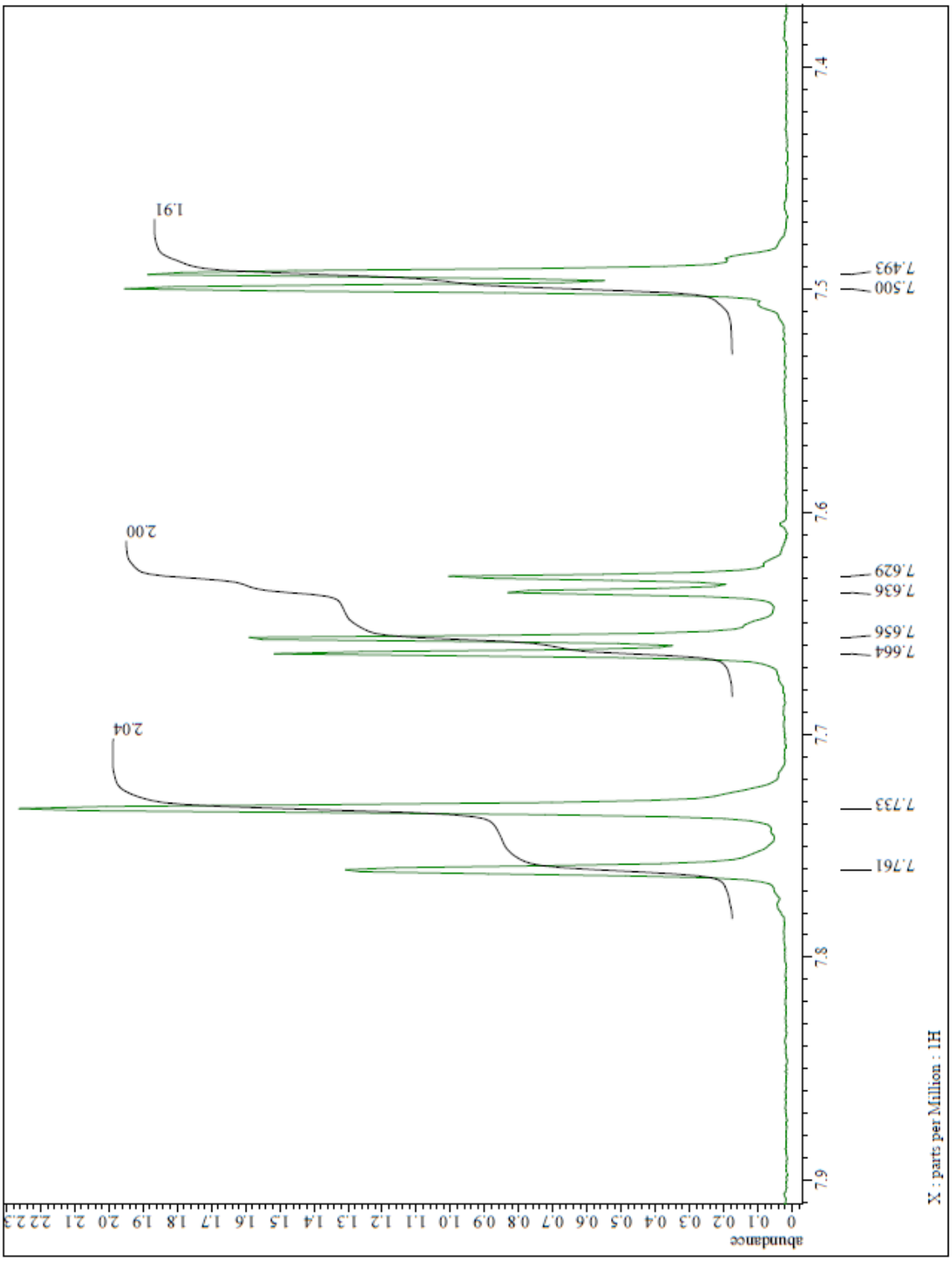

Figure S8. ^{1}H-NMR (300 MHz, $CDCl_3$) **1**

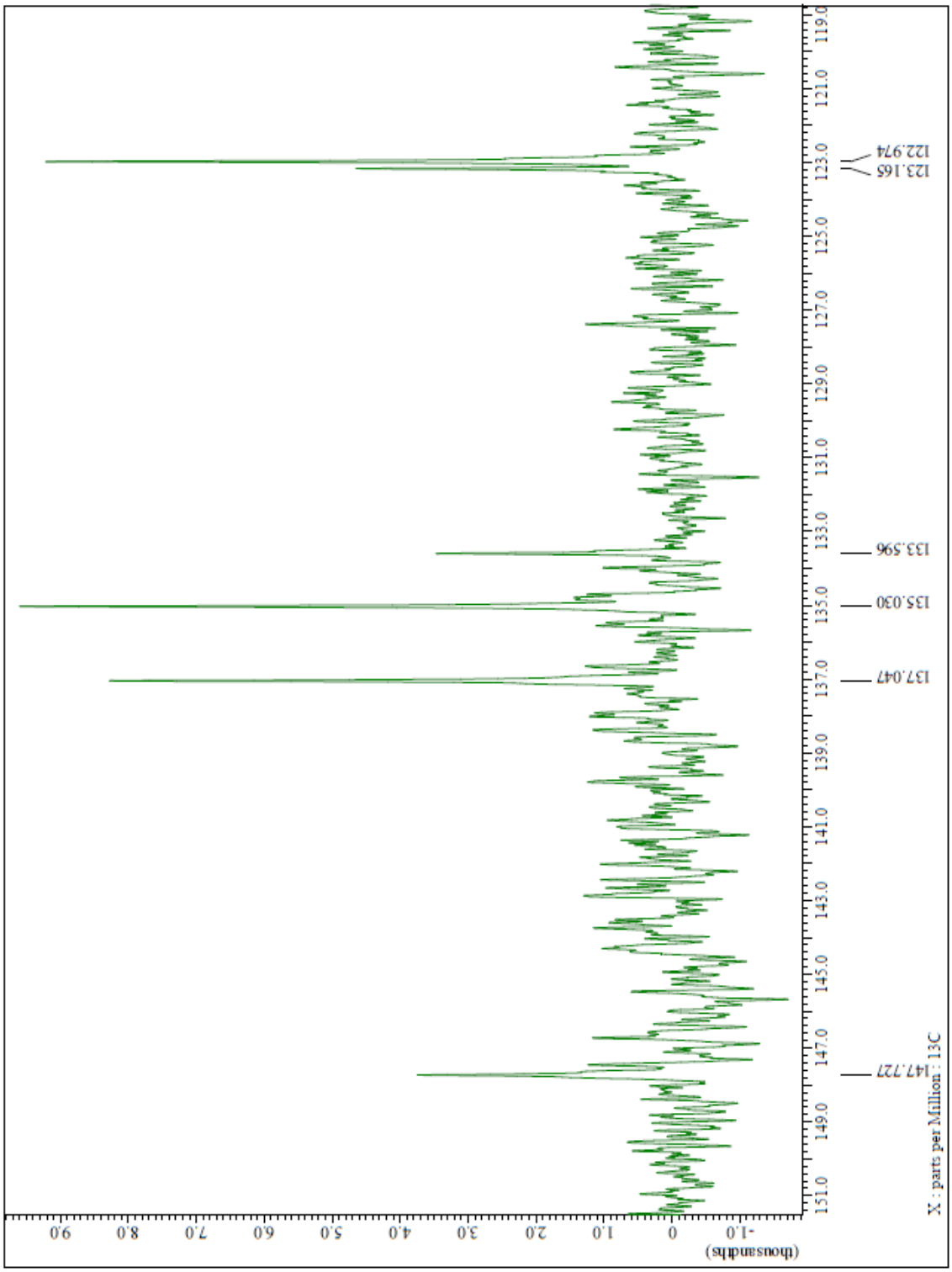

Figure S9. ^{13}C-NMR (300 MHz, $CDCl_3$) of **1**

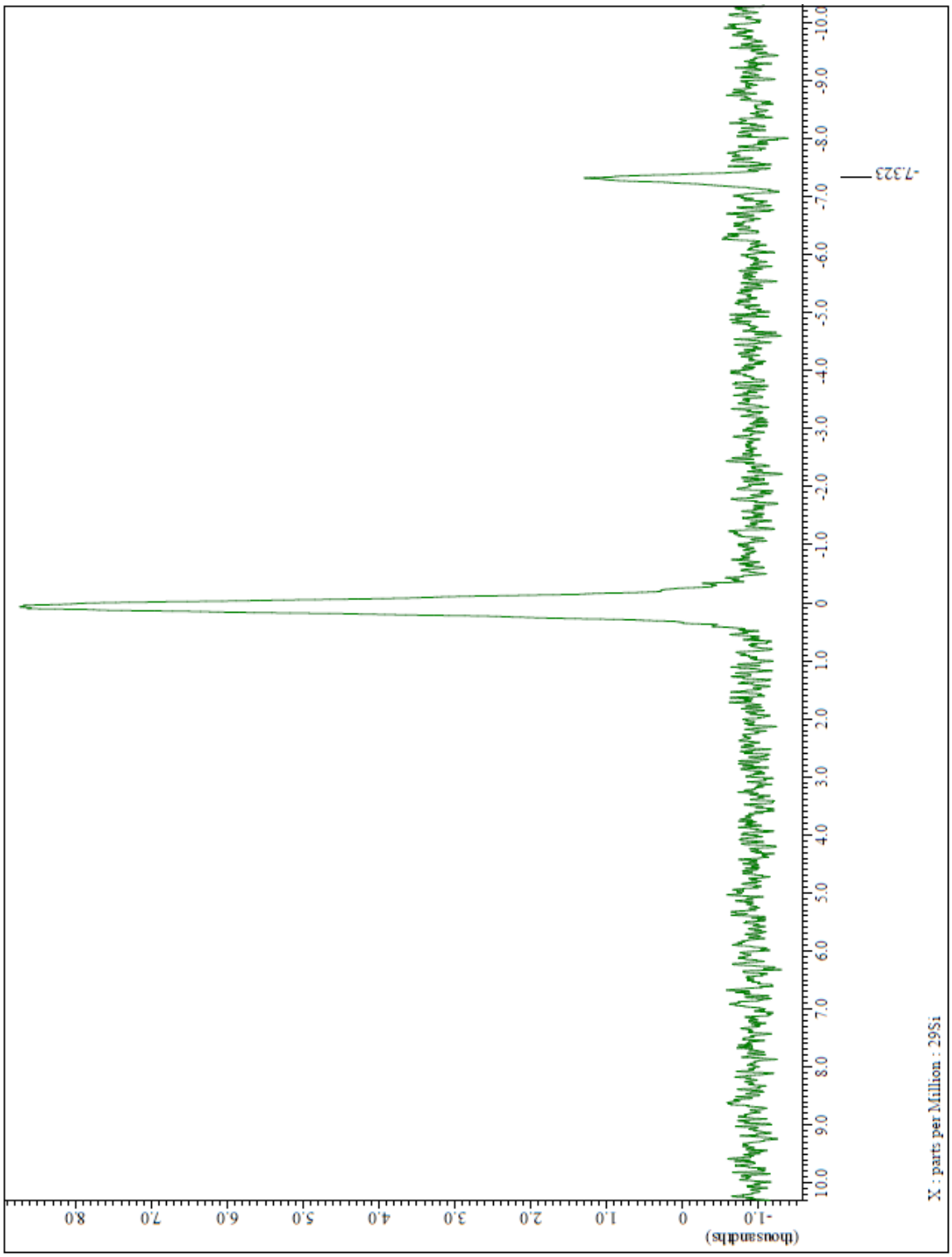

Figure S10. ^{29}Si-NMR (500 MHz, $CDCl_3$) of **1**

Solid state ^{13}C-NMR (CP-MAS at 15kHz) was consistent with amorphous materials. Although, peak broadening precludes direct assignment of peaks, we note the similarities in the aromatic region for **PS1** and **PS1-C**. Both exhibit 4 resolvable peaks in the aromatic region (for **PS1**, δ = 119.9,128.4, 138.8, and 145.8 ppm and for PS1-C, δ = 117.5, 12439, 140.2, and 148.3 ppm). **PS1-C** also has a peak at 65.3 ppm consistent assigned to the quartenary spiro-center. The aromatic region looks qualitatively different for **PS2**, with only 3 resolvable peaks (δ = 126.4, 132.0, and 142.7 ppm).

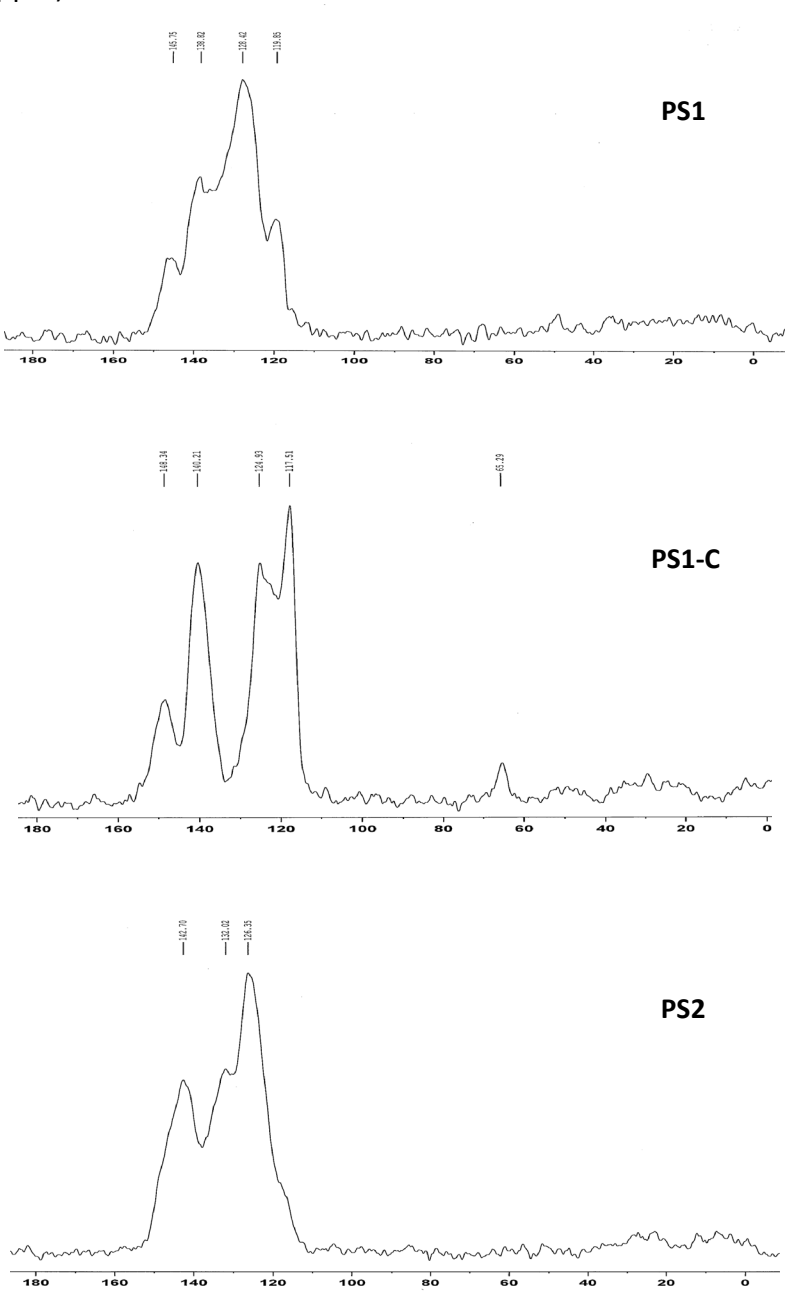

Figure S11. Solid state ^{13}C -NMR (CP-MAS) for condensed networks **PS1**, **PS1-C**, and **PS2**.

Powder XRD spectra of the three condensed networks further indicated that all three materials are amorphous.

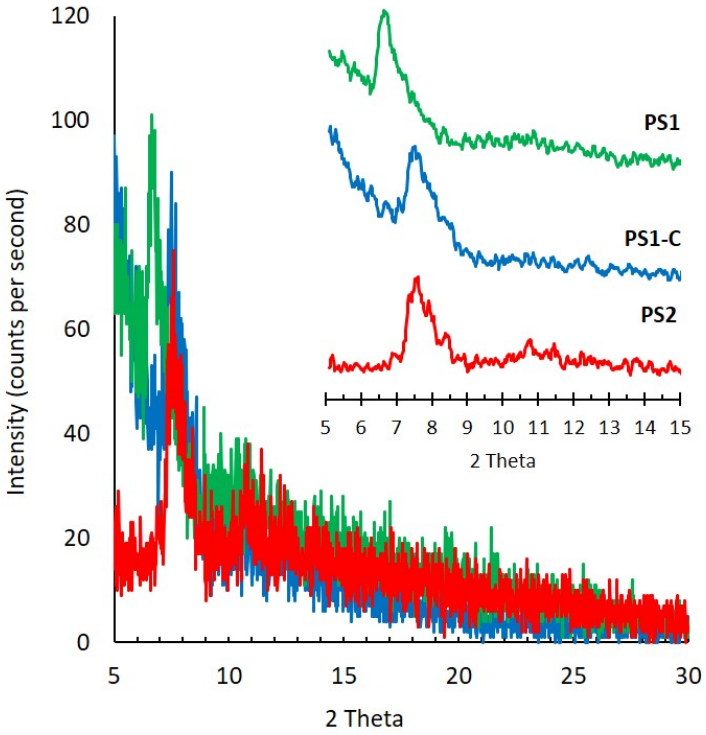

Figure S12. Powder XRD for **PS1** (green), **PS1-C** (blue), and **PS2** (red). Inset shows spectra smoothed and offset.

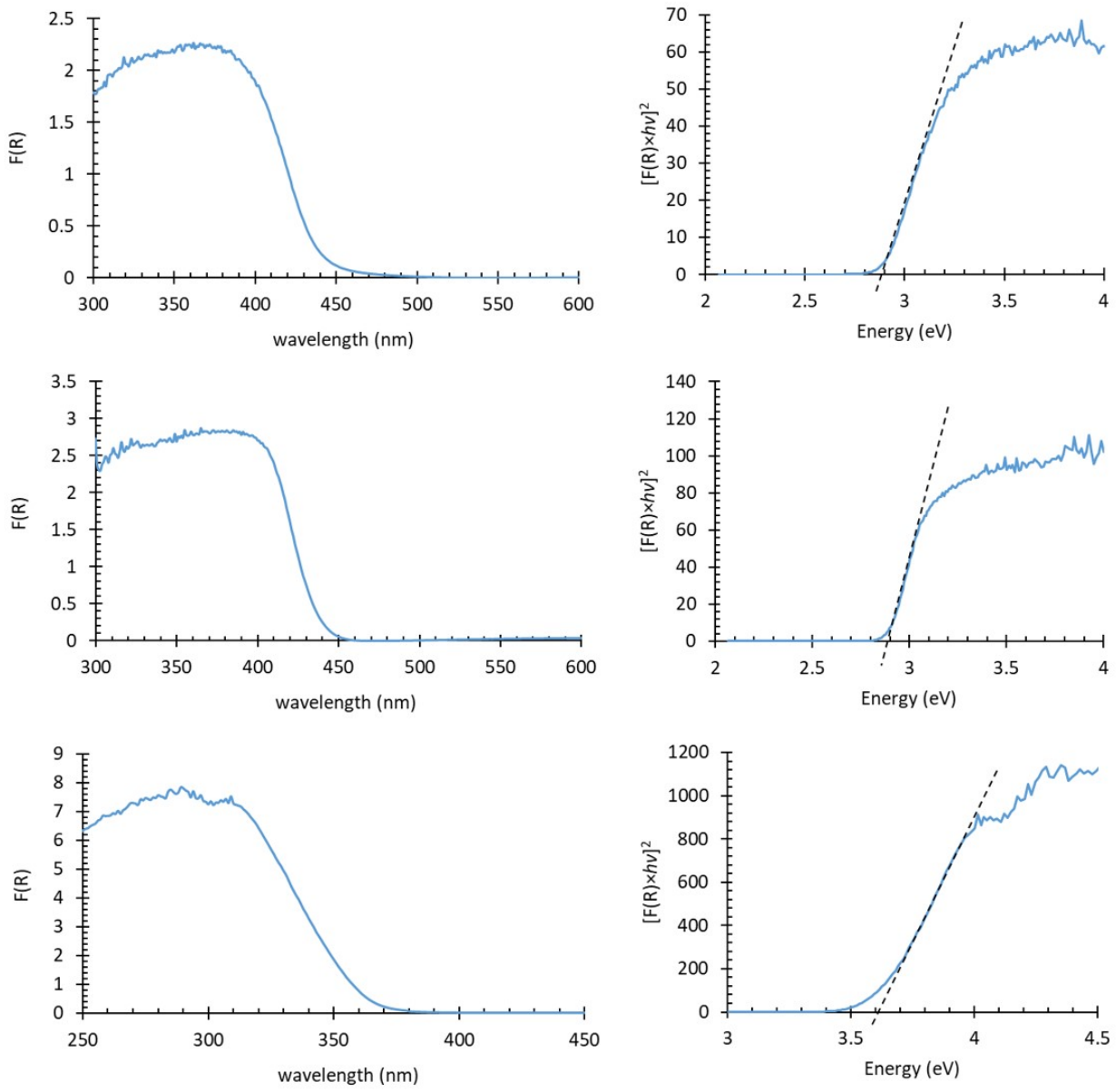

Figure S13. (Left) Diffuse reflectance UV-vis spectra with Kubelka-Munk transform for **PS1** (top), **PS1-C** (middle), and **PS2** (bottom). (Right) Tauc plot, assuming direct allowed gap, for **PS1** (top), **PS1-C** (middle), and **PS2** (bottom).

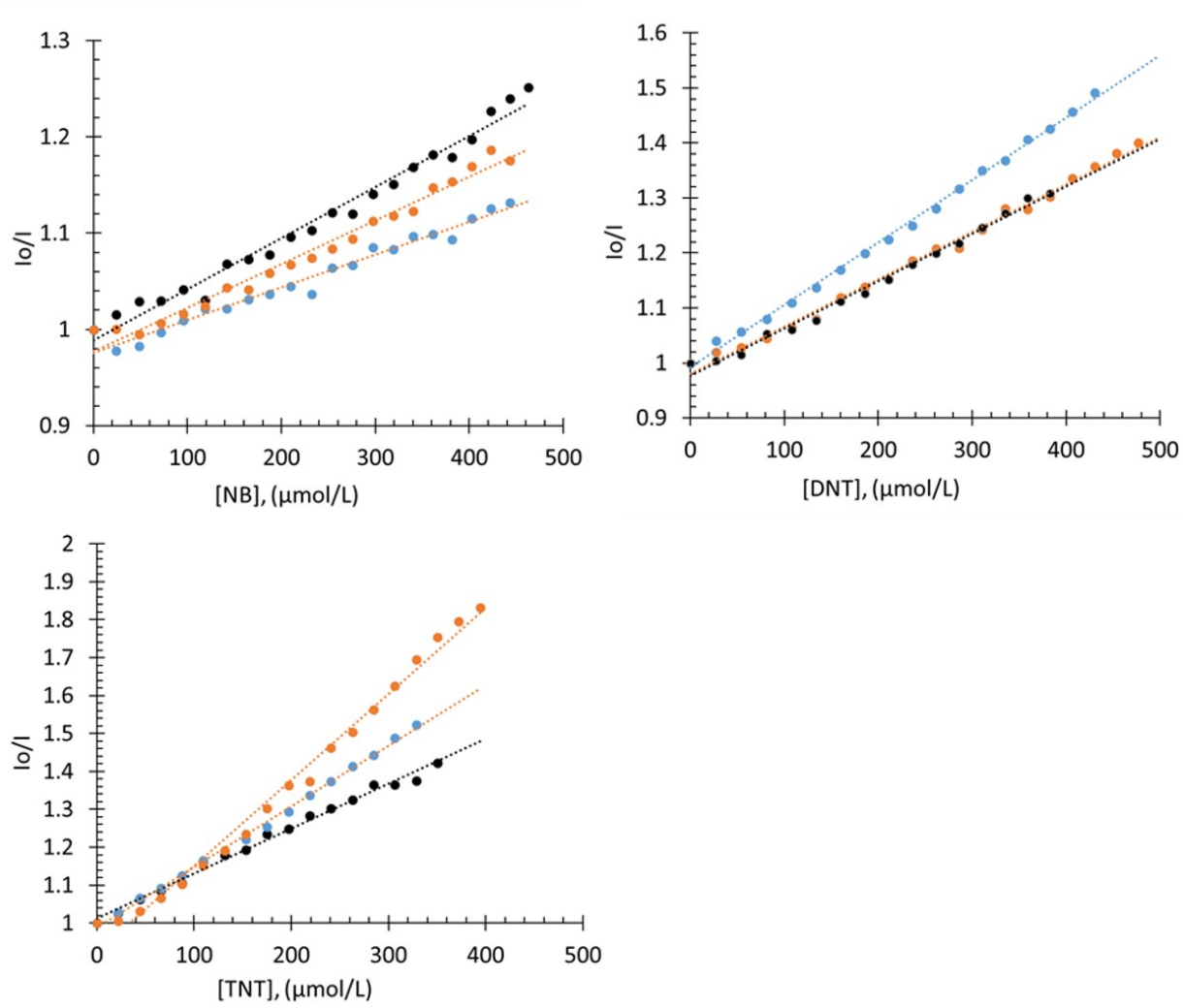

Figure S14. Fluorescence quenching of **PS1** (black), **PS1-C** (orange), and **PS2** (blue) for analytes nitrobenzene (NB), 2,6 -dinitrotoluene (DNT), and 2,4,6-trinitrotoluene (TNT).

Table S2. Results of line fitting for fluorescence quenching experiments

Analyte	Sample	Ksv (L/mol)	R^2	intercept
NB	**PS1**	5.3E+02	0.98	0.99
	PS1-C	4.5E+02	0.98	0.98
	PS2	3.4E+02	0.97	0.98
DNT	**PS1**	8.6E+02	0.99	0.98
	PS1-C	8.6E+02	0.99	0.98
	PS2	1.1E+03	1.00	0.99
TNT	**PS1**	1.2E+03	0.99	1.01
	PS1-C	2.4E+03	0.99	0.92
	PS2	1.6E+03	1.00	0.99

Quenching mechanistic studies: To better understand the quenching mechanism, samples of **PS1** suspended in acetonitrile were quenched with large amounts of nitrobenzene, [nitrobenzene] = 0 – 0.05 mol/L. Even at this high quencher concentration, there is no significant shift in emission as seen in the semi-log plot (Figure S15, insert). At this concentration the Stern-Volmer quenching curve begins to curve upward (Figure S15). The fluorescence lifetime of the samples were also obtained (excitation at 391 nm and monitoring emission at 450 nm). The resulting emission decays were multi-exponential. Each curve was fitted with a 3-exponential fit and the values for the best fit are included in Table S3. An amplitude averaged lifetime, $\langle\tau\rangle_a$, was calculated from these parameters using the equation: $\langle\tau\rangle_a = \sum (a_i \tau_i)/ \sum (a_i)$. The ratio of $\langle\tau_o\rangle_a/\langle\tau\rangle_a$ was then plotted vs. nitrobenzene concentration. The fact that $\langle\tau_o\rangle_a/\langle\tau\rangle_a$ remains very close to 1 as I_o/I approaches 80 indicates that the quenching is primarily static in nature.

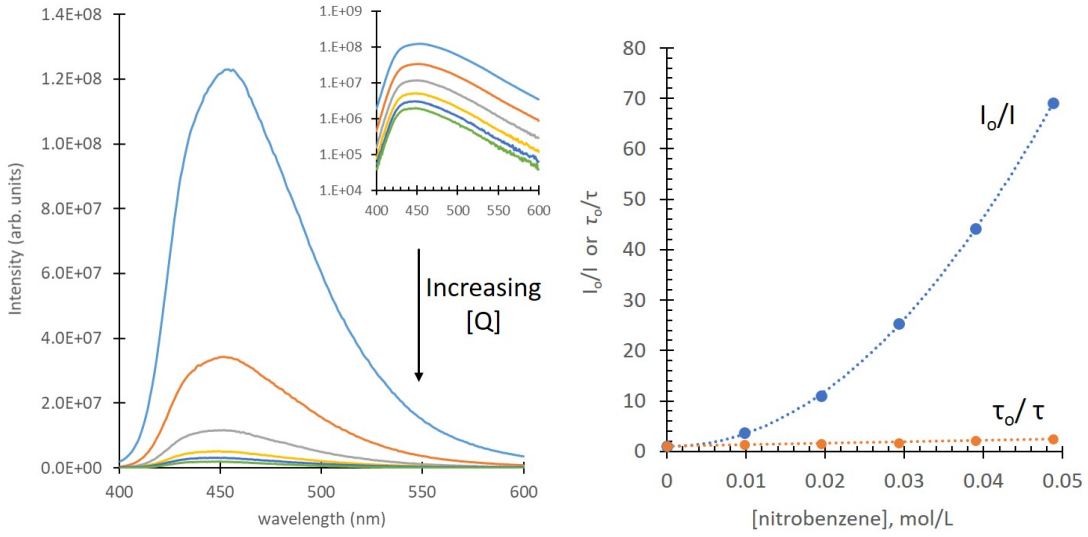

Figure S15. (left) Fluorescence spectrum of **PS1** (blue) in the absence of nitrobenzene quencher, and increasing concentration of nitrobenzene. The insert is a semi-log plot of the same spectra to more clearly indicate the lack of spectral shifting upon quenching. (right) Stern-Volmer plot of I_o/I (blue) and $\langle\tau_o\rangle_a/\langle\tau\rangle_a$ (orange) vs nitrobenzene concentration.

Table S3. Parameters from the best fit of the decay curves using a 3-exponential fit.

[NB], mol/L	t_1 (s)	t_2 (s)	t_3 (s)	a_1	a_2	a_3	$\langle\tau\rangle_a$	$\langle\tau_o\rangle_a/\langle\tau\rangle_a$
0.00E+00	2.18E-10	1.10E-09	3.67E-09	0.643	0.307	0.050	6.62E-10	1.0
9.76E-03	2.09E-10	1.08E-09	4.11E-09	0.730	0.247	0.023	5.12E-10	1.3
1.95E-02	1.65E-10	9.15E-10	3.38E-09	0.746	0.230	0.024	4.16E-10	1.6
2.93E-02	1.94E-10	9.54E-10	3.91E-09	0.798	0.185	0.017	3.97E-10	1.7
3.90E-02	1.23E-10	8.30E-10	3.74E-09	0.806	0.177	0.017	3.11E-10	2.1
4.88E-02	8.53E-11	7.63E-10	3.74E-09	0.809	0.172	0.019	2.70E-10	2.5

In a separate experiment, 0.1 mg of **PS1** was suspended in acetonitrile (2 mL). The solution was sonicated and an initial fluorescence spectrum was obtained. An aliqout of nitrobenzene (0.100 mL) was added to this suspension and a second spectrum was obtained (labeled orange "quenched" in figure S16). The addition of the large excess of nitrobenzene completely quenched the emission of **PS1**. The suspension was then transferred to a beaker. Evaporated to near dryness on a hotplate and then transferred to a vacuum oven where it was heated to 100 ^{o}C for 2 hours. The resulting residue was then resuspended in 2.0 mL of acetonitrile and transferred to a cuvette. The resulting spectrum is labeled gray "recovered" in Figure S16. The partial recovery of fluorescence provides evidence that the quenching is a reversible process although analyte removal from the microporous matrix is challenging.

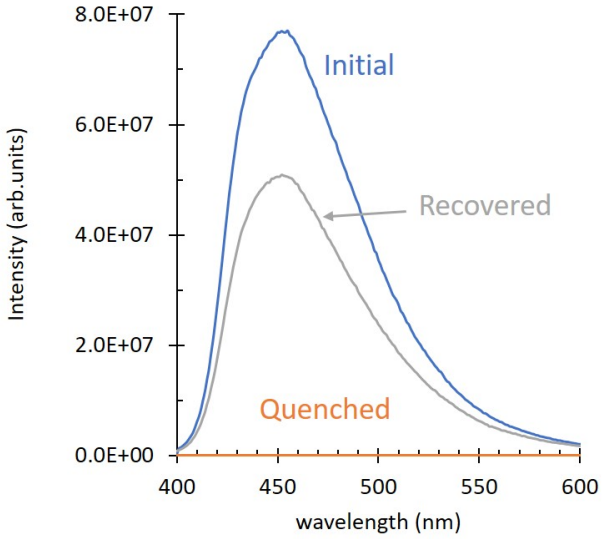

Figure S16. Emission spectrum of (blue) initial suspension of **PS1** in acetonitrile, excited at 370 nm, (orange) upon addition of 0.1 mL of nitrobenzene, and (gray) recovered emission after partial removal of nitrobenzene.

In a separate experiment, samples of **PS1, PS1-C** and **PS2** (approx. 20 mg each) were suspended in 30 mL of acetonitrile and 1 mL of nitrobenzene was added. The suspension was sonicated for two minutes, centrifuged, decanted, and the precipitate was left to dry in a vacuum oven at 80 ^{o}C for 2 hours. These samples were then analyzed using FTIR to look for any identifiable shifts in the IR spectrum (Figure S17). The resulting spectra clearly showed peaks from the nitrobenzene and respective matrix, but there were no obvious shifts in the IR peaks indicating a reaction on the surface. Retention of analyte is clearly evident in all samples following evacuation at 80 ^{o}C (spectra b-d), but heating at 200 ^{o}C under vacuum for 2 hours resulted in complete removal of NB from a sample of **PS1** (spectrum e).

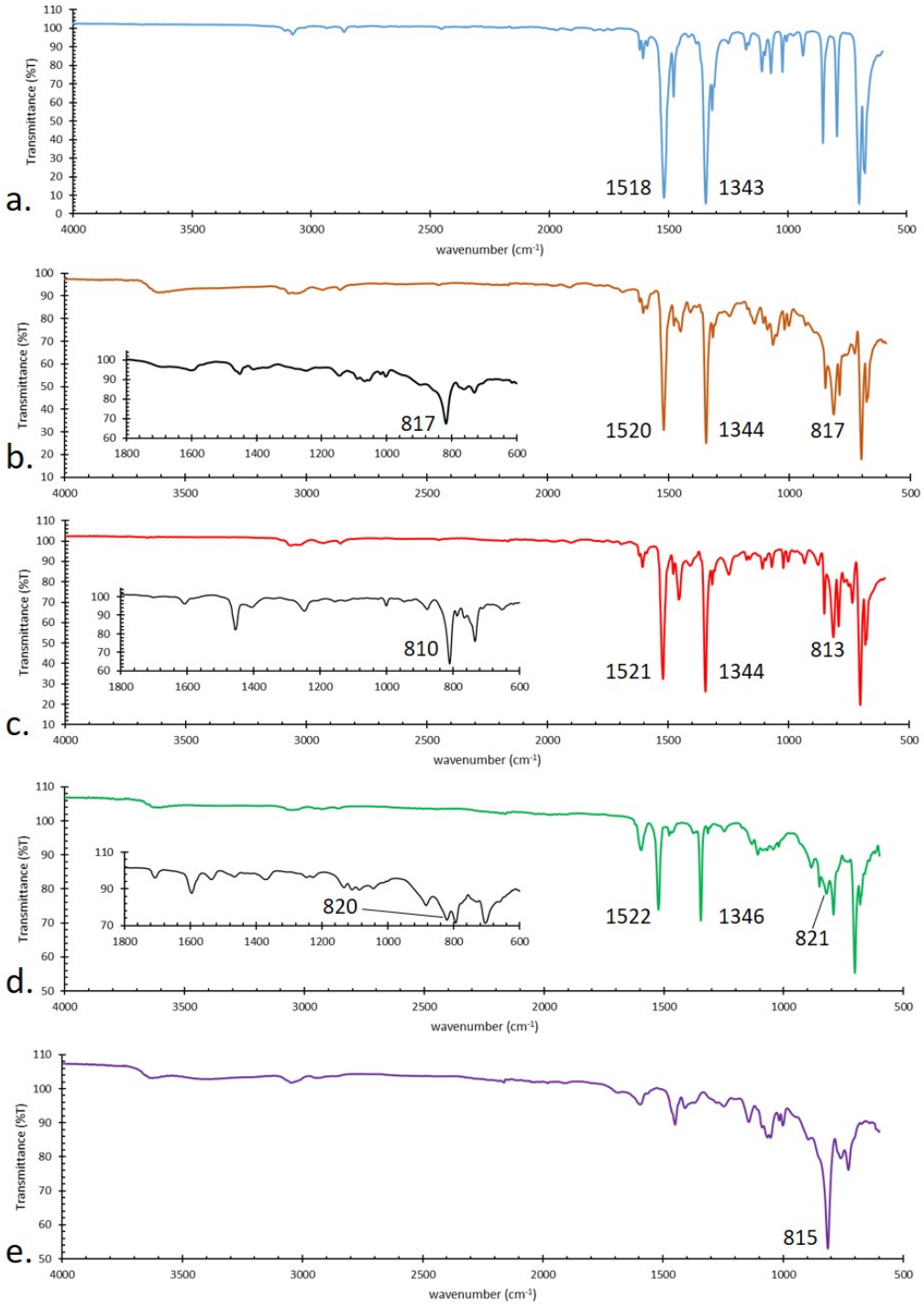

Figure S17. FTIR spectra of (a) nitrobenzene (NB, liquid), (b) **PS1** filled with NB, inset is **PS1** untreated, (c) **PS1-C** filled with NB, inset is untreated **PS1-C**, (d) **PS2** filled with NB, inset is untreated **PS2**, and (e) **PS1** filled with NB then heated to 200 ^{o}C under vacuum for 2 hours.

Adsorption of nitrobenzene did have an effect on the optical properties and tauc plots (Figure S18), which resulted in a slight apparent red-shift of the band gap relative to the pristine samples as shown in Table S4. The samples used for this diffuse reflectance UV-vis study were the same samples used in the FTIR experiments above. Likewise, both samples **PS1** and **PS1-C** appeared more yellow to the eye following saturation with the nitrobenzene. **PS2** remained colorless. The apparent red-shift in the absorbance is consistent with introduction of lower energy interfacial charge transfer bands between the the porous matrix and absorbed quencher and is consistent with a static quenching mechanism.

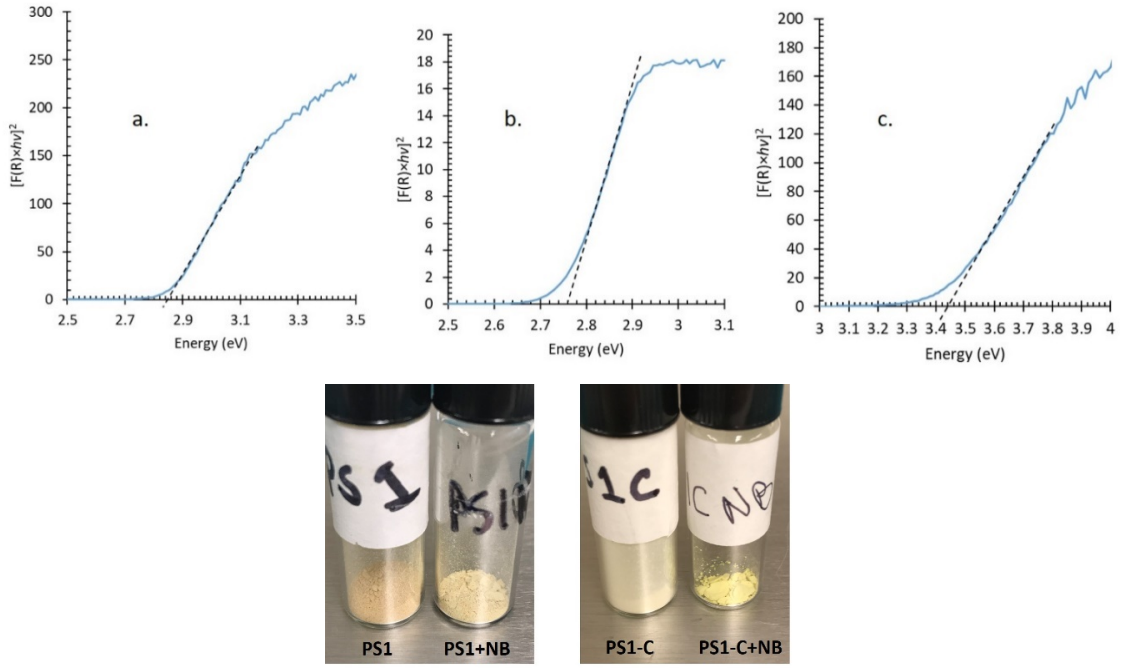

Figure S18. Tauc plots of samples after saturation with nitrobenzene and drying at 80 °C for (a) **PS1**, (b) **PS1-C**, and (c) **PS2**. Photo of (left) **PS1** and (right) **PS1-C** before and after saturation with nitrobenzene.

Table S4.

Sample	Band Gap (eV) With NB	Band Gap (eV) Without NB	Observed shift
PS1	2.85	2.90	-50 meV
PS1-C	2.76	2.90	-140 meV
PS2	3.45	3.61	-160 meV

Finally, we took the sample of **PS1** that had been saturated with nitrobenzene and transferred it to the surface area analyzer. The sample was evacuated and heated to 80 °C overnight prior to obtaining the nitrogen adsorption isotherm shown in Figure S19 top. The same sample was subsequently heated to 200 °C for 2 hours and the nitrogen adsorption isotherm shown in Figure S19 bottom was obtained. Pore analysis data is shown in Figure S20. A summary of the data is shown in Table S5 and is consistent with a strongly adsorbed nitrobenzene quencher that requires extensive heating or dilution for complete removal. An IR spectrum of the sample following evacuation at 200 °C indicated complete removal of nitrobenzene (Figure S17e).

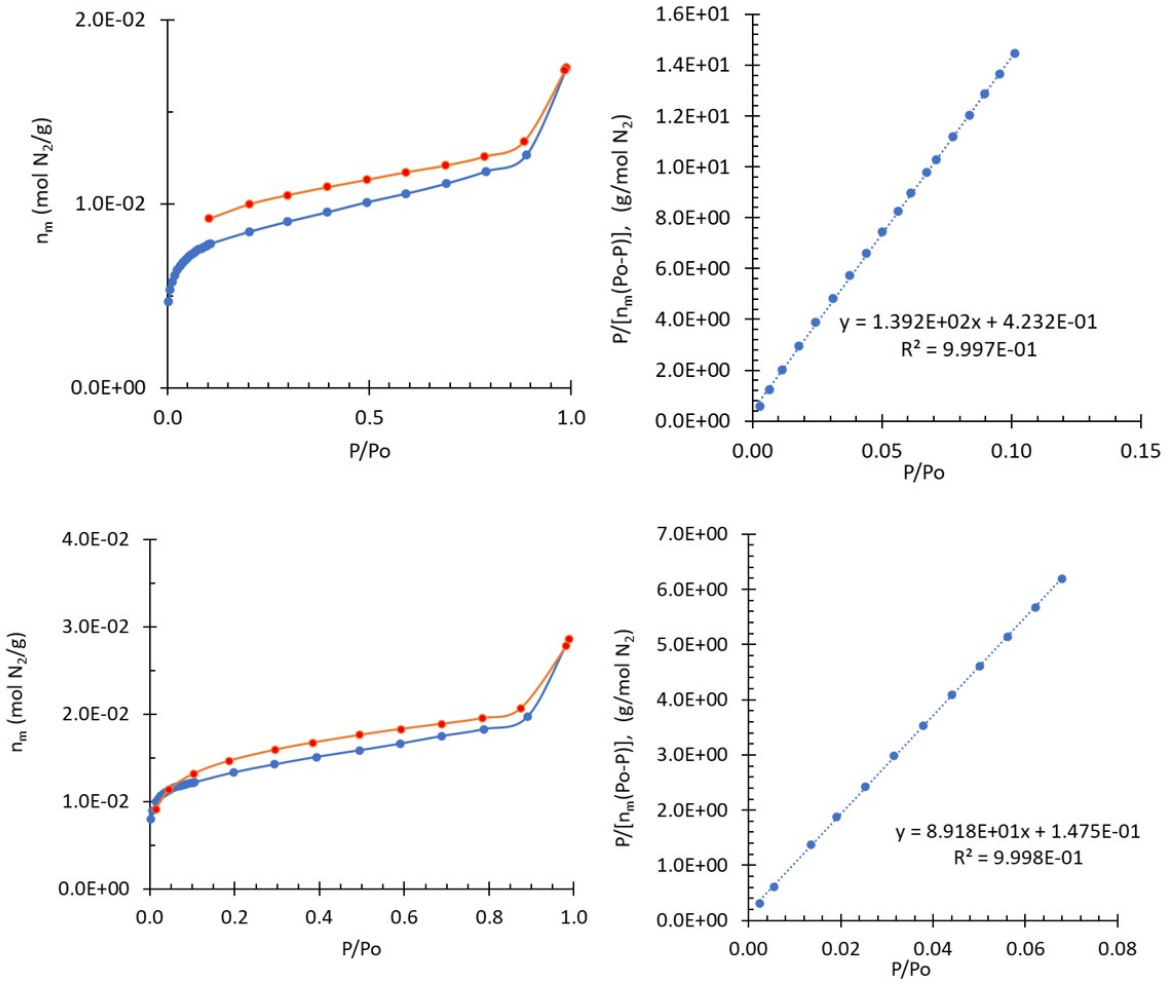

Figure S19. Adsorption isotherms and BET transform plots of microporous region for (top) **PS1** saturated with NB then dried under vacuum at 80 °C overnight and (bottom) the same sample subsequently heated under vacuum to 200 °C for 2 hours.

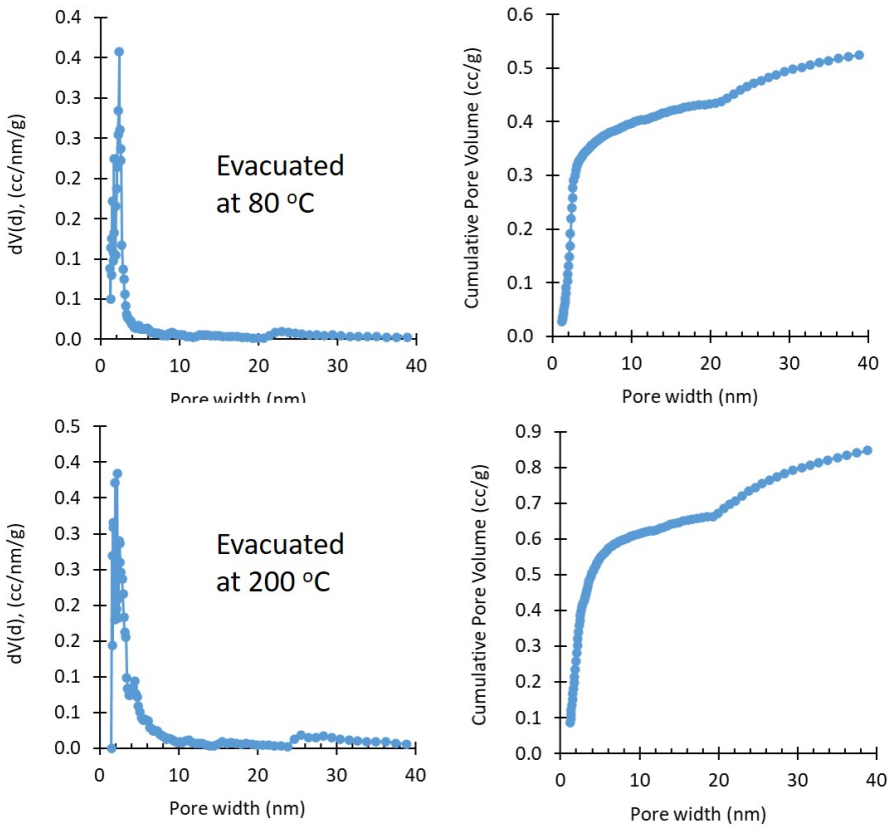

Figure S20. Pore size analysis for (top) **PS1** saturated with nitrobenzene then dried under vacuum overnight at 80 °C and (bottom) same sample following subsequent drying at 200 °C for 2 hours. Calculation model: N_2 at 77 K on carbon (cylindrical pores, NLDFT equilibrium model, Quantachrome NovaWin)

Table S5. Summary of adsorption data following saturation of **PS1** sample with nitrobenzene followed by evaporation under vacuum at 80 °C overnight and at 200 °C for two hours.

Sample	C	n_m, (mol N_2/g)	Surface Area (m^2/g)	**V_{pore} (DFT)** (mL/g)	**Pore Width** (nm)
PS1	268	1.45E-2	1420	1.15	1.7
PS1-NB-80	330	7.16E-3	699	0.55	2.4
PS1-NB-200	606	1.12E-2	1092	0.89	1.7

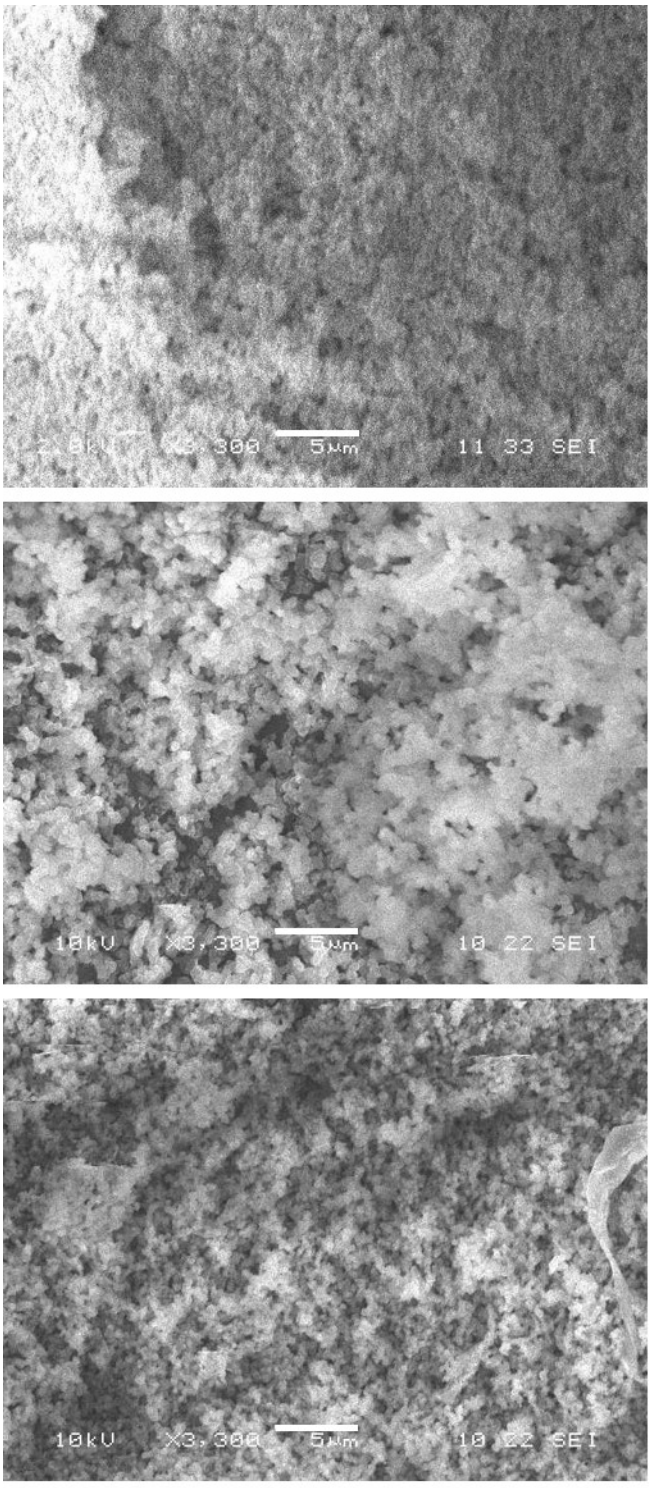

Figure S21. SEM image of condensed materials affixed to copper tape at 3,300 magnification. White bar indicates 5 micrometers.

Computational Modeling

All calculations were performed using Spartan 2016 (SPARTAN '16 Quantum Mechanics Driver: (Win/64b) Release 1.1.0). The **PS1, PS1-C** and **PS2** analog structures were optimized using DFT (B3LYP/6-31G*) in the gas phase.

Table S6. Summary of HOMO and LUMO energy levels of oligomers (n=1-5) of silabifluorene coupled at the 2,7-positions (**PS1 analog**) or 3,6-positions (**PS2 analog**) or the carbon-centered bifluorene coupled at the 2,7 position (**PS1-C analog**).

Si -2,7	**momer**	**dimer**	**trimer**	**tetramer**	**pentamer**
n	**1**	**2**	**3**	**4**	**5**
HOMO	-5.81	-5.43	-5.29	-5.22	-5.18
LUMO	-1.12	-1.44	-1.57	-1.64	-1.68
Eg	4.69	3.99	3.72	3.58	3.5
Si -3,6	**momer**	**dimer**	**trimer**	**tetramer**	**pentamer**
n	**1**	**2**	**3**	**4**	**5**
HOMO	-5.81	-5.74	-5.7	-5.68	-5.67
LUMO	-1.12	-1.42	-1.52	-1.57	-1.58
Eg	4.69	4.32	4.18	4.11	4.09
C-2,7	**momer**	**dimer**	**trimer**	**tetramer**	**pentamer**
n	**1**	**2**	**3**	**4**	**5**
HOMO	-5.64	-5.36	-5.2	-5.14	-5.1
LUMO	-0.79	-1.21	-1.4	-1.46	-1.5
Eg	4.85	4.15	3.8	3.68	3.6

HOMOs and LUMOs representations of pentameric structures of PS1, PS1-C and PS2 analogs are included below.

HOMOs

PS1

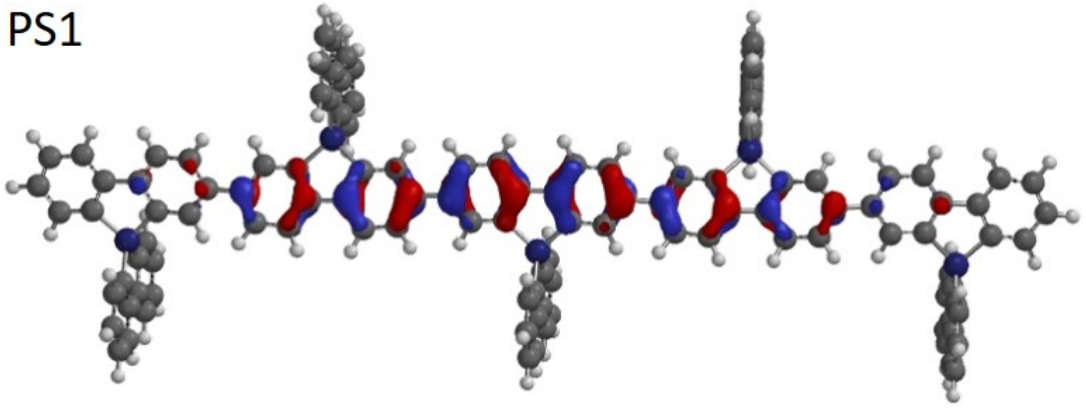

PS1-C

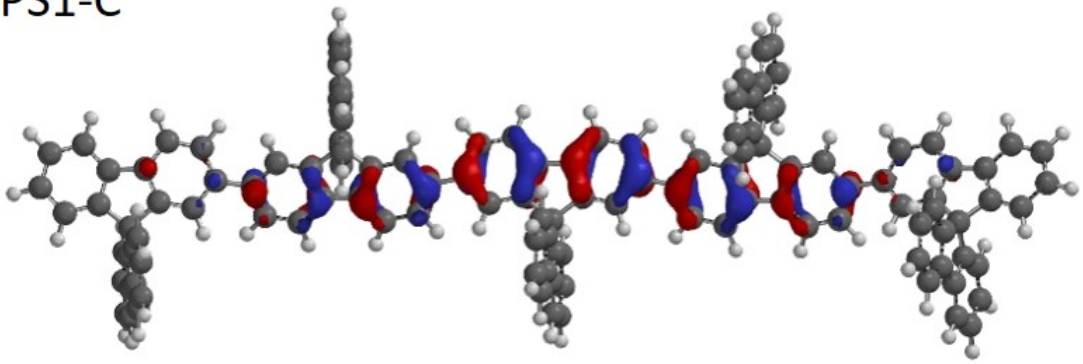

PS2

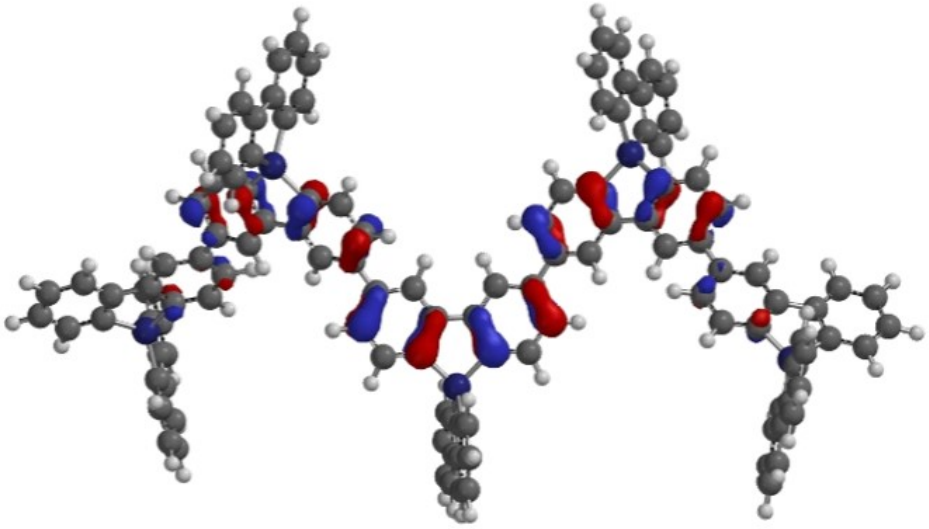

LUMOs

PS1

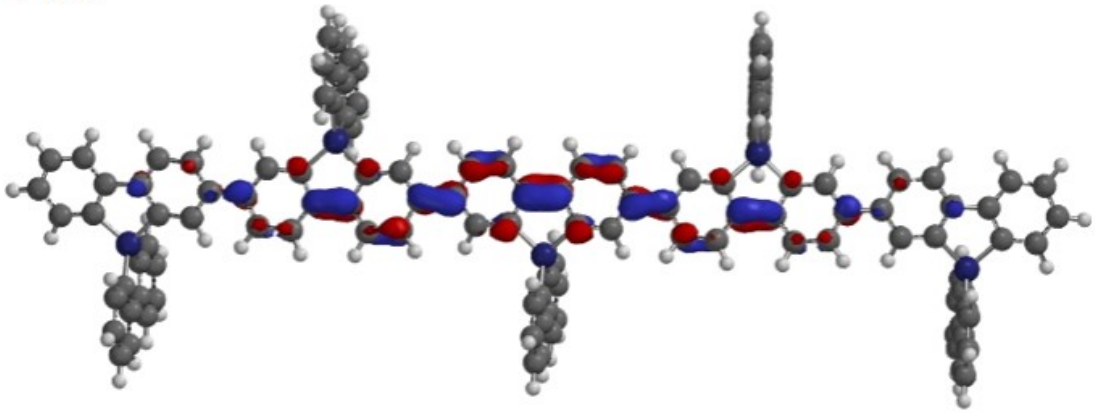

PS1-C

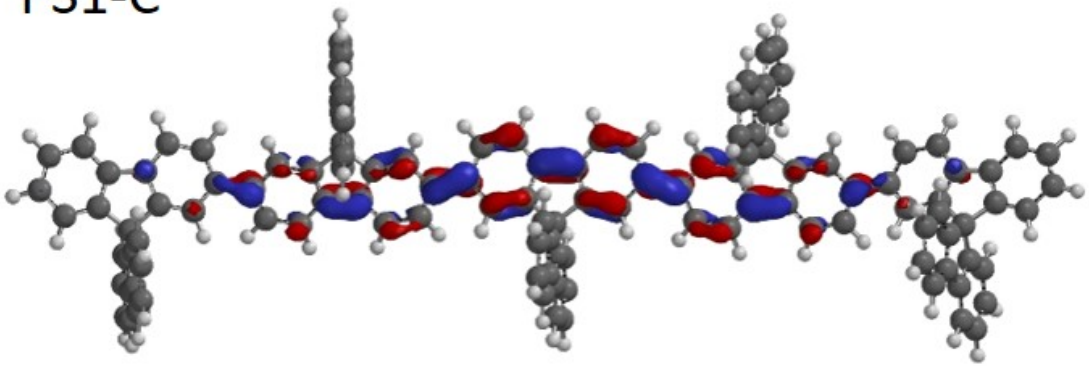

PS2

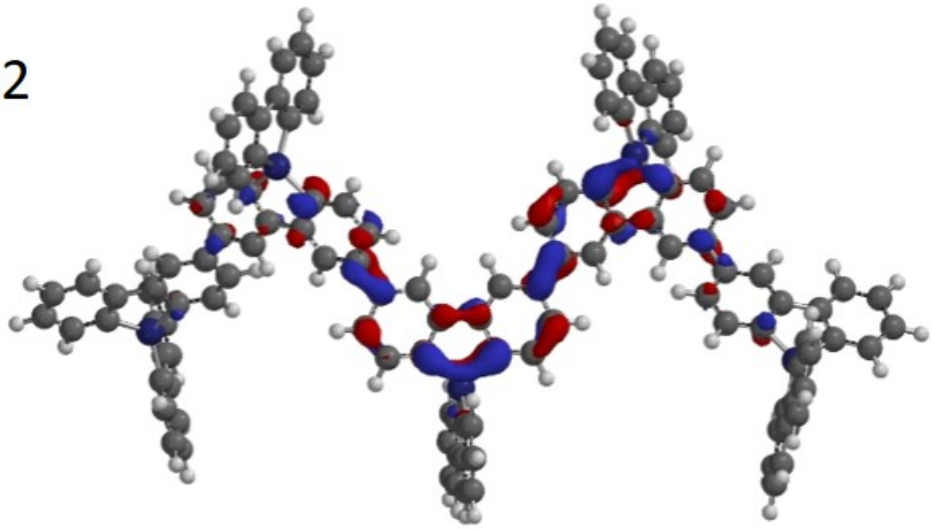

Table S7. Crystal data and structure refinement for Structure **1**, (CCDC #1995230).

Empirical formula	C_{31} H_{20} Br_4 Si	
Formula weight	740.20	
Temperature	100(1) K	
Wavelength	1.54184 Å	
Crystal system	Triclinic	
Space group	P-1	
Unit cell dimensions	a = 11.1507(8) Å	= 74.098(5)°.
	b = 11.5156(6) Å	= 80.106(6)°.
	c = 11.6809(8) Å	= 83.183(5)°.
Volume	1416.99(16) $Å^3$	
Z	2	
Density (calculated)	1.735 Mg/m^3	
Absorption coefficient	7.476 mm^{-1}	
F(000)	720	
Theta range for data collection	3.98 to 67.17°.	
Index ranges	-10<=h<=13, -13<=k<=13, -12<=l<=13	
Reflections collected	14024	
Independent reflections	5027 [R(int) = 0.0388]	
Completeness to theta = 67.17°	99.2 %	
Refinement method	Full-matrix least-squares on F^2	
Data / restraints / parameters	5027 / 0 / 326	
Goodness-of-fit on F^2	1.069	
Final R indices [I>2sigma(I)]	R1 = 0.0326, wR2 = 0.0853	
R indices (all data)	R1 = 0.0354, wR2 = 0.0877	
Largest diff. peak and hole	0.577 and -0.830 $e.Å^{-3}$	

Table S8. Crystal data and structure refinement for Structure **2**, (CCDC #1995231).

Empirical formula	C_{24} H_{12} Br_4 Si	
Formula weight	648.07	
Temperature	106(8) K	
Wavelength	1.54184 Å	
Crystal system	Orthorhombic	
Space group	P b c a	
Unit cell dimensions	a = 10.3068(2) Å	□= 90°.
	b = 14.7409(2) Å	□= 90°.
	c = 28.6394(4) Å	□ = 90°.
Volume	4351.23(12) $Å^3$	
Z	8	
Density (calculated)	1.979 Mg/m^3	
Absorption coefficient	9.622 mm^{-1}	
F(000)	2480	
Crystal size	0.200 x 0.108 x 0.076 mm^3	
Theta range for data collection	5.288 to 67.083°.	
Index ranges	-10<=h<=11, -17<=k<=17, -34<=l<=34	
Reflections collected	94225	
Independent reflections	3867 [R(int) = 0.0353]	
Completeness to theta = 67.083°	99.3 %	
Refinement method	Full-matrix least-squares on F^2	
Data / restraints / parameters	3867 / 0 / 263	
Goodness-of-fit on F^2	1.158	
Final R indices [I>2sigma(I)]	R1 = 0.0177, wR2 = 0.0443	
R indices (all data)	R1 = 0.0183, wR2 = 0.0446	
Extinction coefficient	0.000088(9)	
Largest diff. peak and hole	0.472 and -0.285 e.$Å^{-3}$	

References:

1. M. Thommes, K. Kaneko, A. V. Neimark, J. P. Olivier, F. Rodriguez-Reinoso, J. Rouquerol and K. S. W. Sing, *Pure and Applied Chemistry*, 2015, **87**, 1051-1069.
2. Rigaku Oxford Diffraction, (2018), CrysAlisPro Software System, version 1.171.38.46, Rigaku Corporation, Oxford, UK.
3. G.M. Sheldrick, *Acta Cryst.* 2008, **A64**, 112-122.
4. O. V. Dolomanov, L. J. Bourhis, R. J. Gildea, J. A. K. Howard and H. Puschmann, *J. Appl. Cryst*. 2009, **42**, 339-341.
5. K. L. Chan, S. E. Watkins, C. S. K. Mak, M. J. McKiernan, C. R. Towns, S. I. Pascu and A. B. Holmes, *Chemical Communications*, 2005, 5766-5768.
6. C. W. Keyworth, K. L. Chan, J. G. Labram, T. D. Anthopoulos, S. E. Watkins, M. McKiernan, A. J. P. White, A. B. Holmes and C. K. Williams, *Journal of Materials Chemistry*, 2011, **21**, 11800-11814.
7. B. G. Hauser, O. K. Farha, J. Exley and J. T. Hupp, *Chemistry of Materials*, 2013, **25**, 12-16.